Modelling debris distribution of masonry panels subject to blast loads using experimental & applied element methods

Richard A. Keys, PhD Researcher[1], Simon K. Clubley, Lecturer in Civil Engineering[1]

[1]Infrastructure Group, Faculty of Engineering and the Environment
University of Southampton, Southampton

May 2013

Abstract

Blast loading and its interaction with structures is a complex phenomenon even in the simplest of cases and modelling its effects is a non-trivial task. This complexity is increased when dealing with long duration blast due to the drag loads associated with the dynamic pressure.

This paper establishes a scientific benchmark for the debris distribution modelling of masonry panels as the foundation of an extended in-depth research study. Experimental trials were conducted in which identical masonry walls were subjected to separate conventional high explosive and long duration blast loads for comparison. Both experiments were subsequently modelled using the Applied Element Method (*AEM*) with the computational results demonstrating good agreement. The experimental blast loads were characterised with matching overpressures for computational simplicity allowing for a direct comparison between both cases and a clear indication of the effects of impulse, dynamic pressure and entrainment on debris distribution.

Introduction

The work summarised in this paper forms a scientific basis on which a longer in-depth research projected will be conducted. This research aims to develop a set of algorithms to predict the breakage and debris distribution for a large variety of simplified masonry structures when subjected to long duration blast loads. Long duration blast loading is identified here as an explosive event in which the positive phase duration exceeds 100ms and is most commonly associated with hydrocarbon vapour cloud detonation, such as the 2005 'Buncefield Disaster' [1] and the more recent 2013 'Texas Fertilizer Plant Disaster,' or large scale explosive detonations such as the 1981 'Mill Race' Trial [2].

By nature, long duration blast waves transmit very large impulses and the non-negligible effects of drag loads associated with the dynamic pressure make its interactions and effects much more complex to model than the conventional case. To develop a modelling routine capable of accurately simulating structural response to such effects, the procedure must be applied to the conventional case to gauge its performance and appropriateness.

When modelling structural collapse the reliability of some numerical methods such as Finite Element Analysis (*FEA*) break down in the discrete phase, especially when modelling brittle materials which are susceptible to particulate breakage. It is difficult to accurately model the kinematic and ballistic interactions of the elements in this phase using nodal connections. Other numerical methods however model the element connections through alternative approaches such as the Applied Element Method (*AEM*). AEM uses face connecting springs with collision detection allowing elements to re-contact other elements during the discrete phase, thus allowing for a reliable model of the debris distribution of such failures.

The collisions between elements during the discrete phase are automatically detected and modelled by temporary shear springs and normal springs. These collisions are modelled differently depending on the type of contact made, as shown in Figure 1, which illustrates the

direction of the springs in edge-to-edge contact and the ability to model multiple element collisions [3, 4].

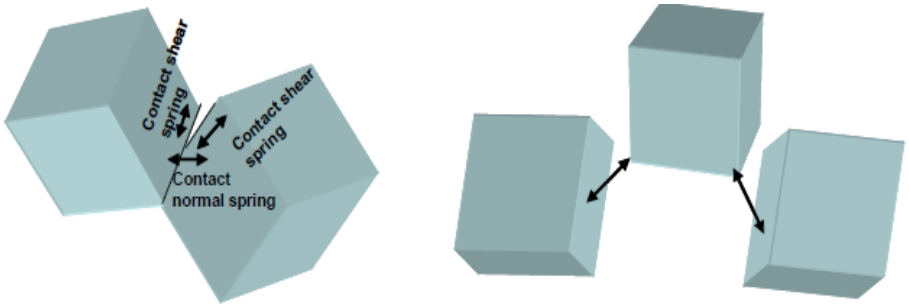

Figure 1. AEM Element Collisions [3, 4]

Methodology

This research uses conventional blast testing to develop a modeling routine using AEM to model the breakage and debris distribution of masonry. Once this routine has been established it will be adapted to incorporate long duration blast loads.

Experimental

The conventional HE tests utilised a 41kg TNT eq. charge composed of 39kg of TNT-Flake boosted by 2kg of PE-4, situated 1m above ground level resulting in an almost hemispherical blast wave. Five identical masonry walls of 2m height × 1m width were placed on radial spokes at distances designed to achieve the overpressures listed in Table 1. These radial spokes and their corresponding peak overpressures, reflected pressures, impulses, arrival times and positive phase durations as calculated using the Kingery & Bulmash Equations [5], are listed in Table 1.

r (m)	P_i (kPa)	I_i (kPa.ms)	P_r (kPa)	I_r (kPa.ms)	t_a (ms)	t^+ (ms)
10.6	110	313	310	752	12.8	10
13	73	262	186	595	18.1	11.5
15	55	231	134	505	22.9	12.3
19.5	35	183	80	378	34.2	13.7
36	14	103	30	195	78.8	16.7

Table 1. Masonry Wall Positions & Parameters for a Hemispherical Surface Burst

The walls were constructed from frogged, facing, London bricks approximately 2.1kg each with an average compressive strength of 4-6N/mm^2. The bricks were joined by a class (ii) mortar in accordance with BS:5628-1:2005 [6], with an average compressive strength of 8-10N/mm^2 (at the time of firing) and a bedding thickness of approximately 1cm. The walls were painted and each brick was numbered to determine the rough origin of the debris. Grids were sprayed around each wall with a bin resolution of 50cm × 50cm for debris collection. Endevco 8510 gauges were placed matching the radial positions of the walls to measure the static overpressure. High speed Phantom photography capturing 5000fps was used to record the breakage of the walls at the 10.6m and 13m positions from different angles.

Figure 2 illustrates a plan view of the trial arrangement and displays the exact positions of the walls. Preliminary models showed that this arrangement would not cause any significant interference between the walls.

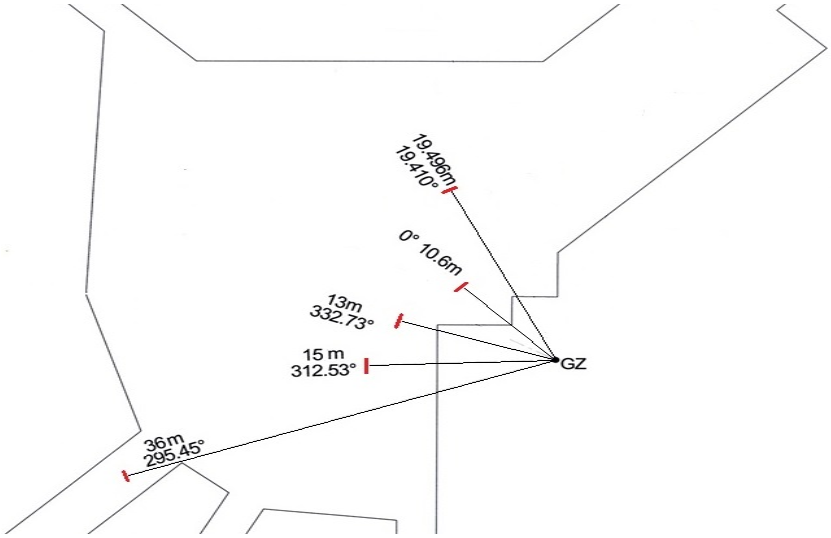

Figure 2. Schematic Diagram of Experimental Layout

The *ABT* (Air Blast Tunnel) facility at MOD Shoeburyness on Foulness Island is capable of simulating long duration blast waves replicating those of large conventional HE charges [7]. A masonry panel of the same 2m × 1m construction was placed in the ABT and subjected to a blast wave with a peak incident overpressure of $P_i \approx 110$kPa and positive phase duration $t^+ \approx 200$ms. Using the Kingery & Bulmash equations [5], this can be attributed to roughly a 500T TNT eq. burst at 250m. Free field pressure gauges were placed around the wall offset in the upstream direction by roughly 1m along with a dynamic pressure gauge. Two high speed phantom cameras capturing at 5000fps were used to record the breakage of the wall from both the upstream and side-on position.

Computational

Numerical modelling was conducted using the software Extreme Loading for Structures® (*ELS*) which utilises AEM. Preliminary computational analyses were run to resolve some of the unknown quantities and parameters. Using the Comutational Fluid Dynamics (*CFD*) code Air3D (v.9) [8], a parametric study was conducted to examine uniformly distributed gauge points on both faces of the walls.

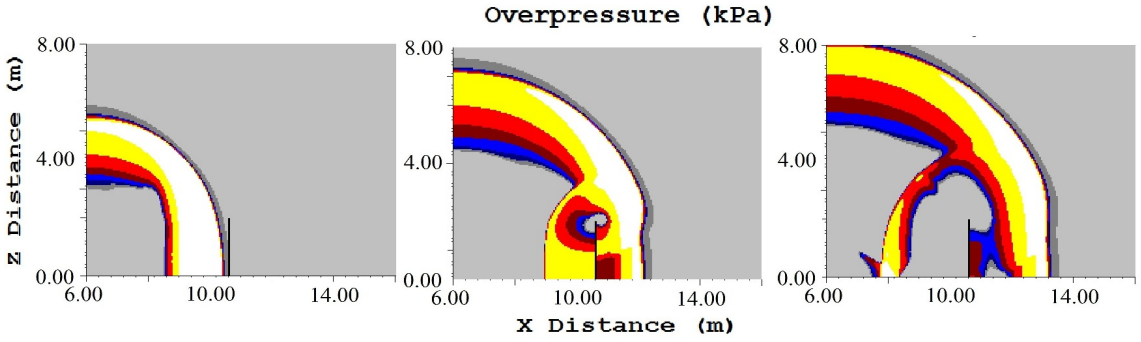

Figure 3. Air3D Model Displaying the Propagation of the Blast Wave over the Wall at 10.6m (10.8-17.6ms)

The first image in Figure 3 shows that upon reaching the 10.6m position there is still a significant curvature in the expansion of the wave with respect to the height of the wall. As a result, the wall is subjected to a non-uniform load which is accentuated by the clearing of

the blast wave and the subsequent rear loading. To accurately recreate the breakage and hence debris distribution this must be taken into account.

Using Air3D a total of 100 gauge points were uniformly placed across both faces of the walls; each gauge occupying a 20cm × 20cm area. From each gauge point the transmitted impulse is calculated and plotted. Figures 4a and 4b show the loading regions on the front and rear of the wall.

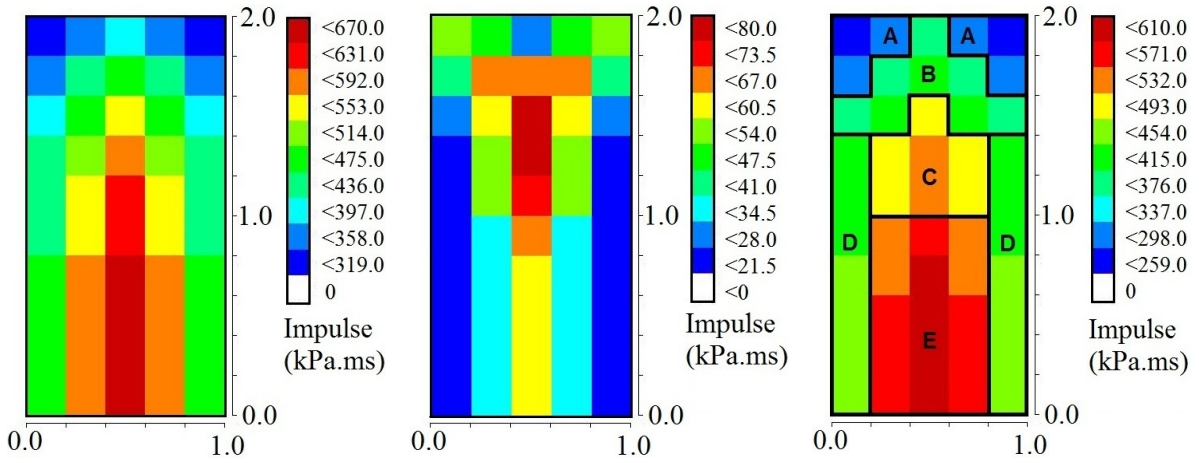

(a) Front Load **(b)** Rear Load **(c)** Net Load & Loading Regions

Figure 4. Load Distribution of the Wall at 10.6m

The impulse scale in Figure 4b shows the rear loading effect of the blast wave is between 20-80kPa.ms. This leads to a 6-25% reduction in the overall loading of the structure and is therefore vital that it is resolved. Furthermore, referring back to Figure 3, it can be seen that whilst the negative phase acts upon the front of the wall, the positive phase is still in effect on the rear of the wall, with both forces acting in the same direction. Figure 4c shows the effective net load obtained by subtracting the rear impulse from the front. The sections labelled from A to E highlight the regions to which the load will be divided within the AEM model. These regions were identified primarily based upon transmitted impulse; however, the arrival time of the blast wave at each region was also considered. This routine for identification of the loading regions is used for all models subjected to conventional blast. For this particular test all of the walls that were tested are identical; thus each simulation developed using AEM uses the same structural model with a different application of load.

Whilst this modelling routine offers promising results for the conventional case, the long duration case requires a different approach. Due to computational restrictions relating to the domain and cell size there is currently no access to a CFD model for such a high yield event. Applying the Kinergy & Bulmash equations [5] to the long duration case, it can be seen from Table 2 that for the long duration case both the incident and reflected impulses are roughly 20 times higher than for the conventional case. As a result the wall is quickly overmatched which creates difficulties in assessing the significance of the various loads.

Q (kg)	r (m)	P_i (kPa)	I_i (kPa.ms)	P_r (kPa)	I_r (kPa.ms)	t_a (ms)	t^+ (ms)
41	10.6	110	313	310	752	12.8	10
5×10^5	250	105	7052	290	16822	306.3	233.7

Table 2. Comparison of Conventional & Long duration Blast Parameters

The preliminary modelling for the long duration case will rely on the experimental gauge data which is in limited supply. The initial models apply the load instantaneously to every element of the wall as the blast wave is planar.

Results & Analysis

Experimental

Due to the circular cross section and relatively small radius of the ABT, the debris was collected in one dimensional longitudinal bins of width 1m. The one dimensional mass distribution data from each bin was extrapolated into 2D by fitting each bin to a Gaussian distribution with a mean value of $\mu = 0$ and a standard deviation of $\sigma = 1$ (standard normal distribution), as shown in Equation 1.

$$f(m, x) = m\frac{1}{\sqrt{2\pi}}e^{-\frac{x^2}{2}} \tag{1}$$

This data was then plotted as shown in Figure 5a for comparison with the conventional case shown in Figure 5b. Figure 5c shows the same data as Figure 5b, plotted on a different scale to show the localised mass distribution.

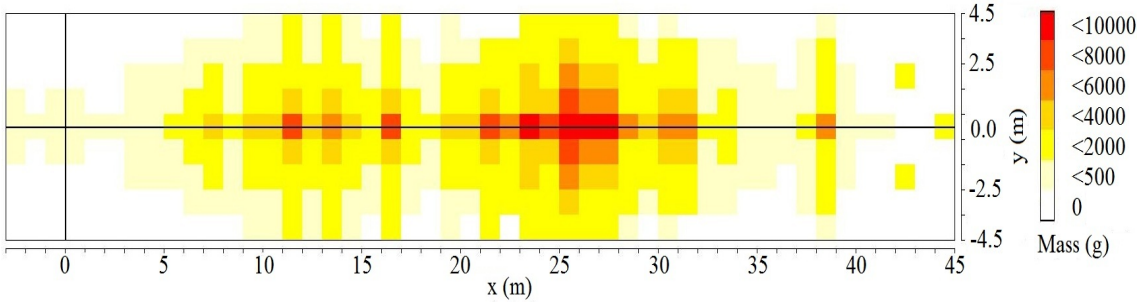

(a) 500T at 250m - Mass Normalised to 10kg

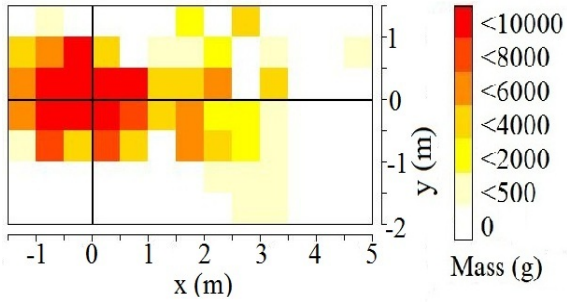

(b) 41kg at 10.6m - Mass Normalised to 10kg

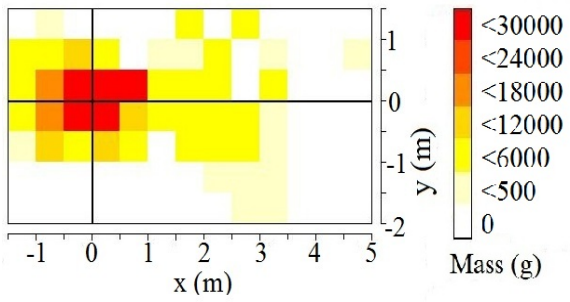

(c) 41kg at 10.6m - Mass Normalised to 30kg

Figure 5. Experimental Debris Mass Distribution Plots for $P_i \approx 110$kPa

Figure 5 demonstrates the maximum longitudinal throw distance of the debris for the long duration case is roughly 8 times that of the conventional case. The gauge data, as displayed in Figure 6, shows that the long duration event transmits over 20 times the free field impulse to that of the conventional case. Furthermore, impulse associated with the dynamic pressure in the long duration case which can interact with ballistic debris is 3 times higher than the conventional free field impulse. This illustrates the vastly increased loading potential and complexity of long duration blast.

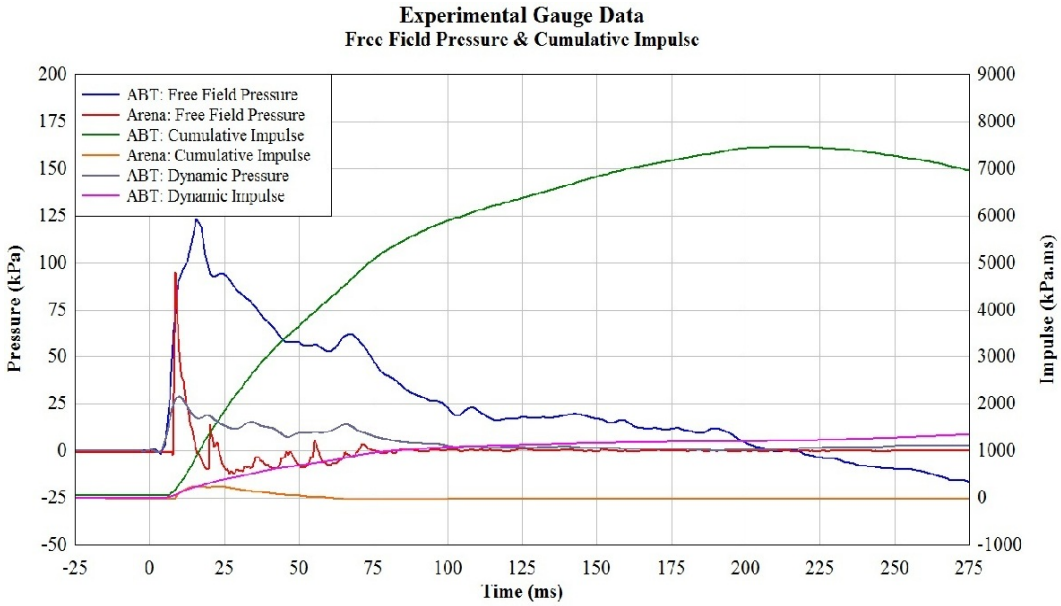

Figure 6. Experimental Free Field (& Integrated) Gauge Data

Results shown in Figure 6 are in good agreement with the predictions shown in Table 2. The results displayed in Figures 5 and 6 demonstrate the requirement for the development of a reliable relationship between the transmitted impulse, peak overpressure and spatial debris distribution for masonry.

Computational

In the early stages of this research project, time constraints have allowed for a restricted number of models. After some refinements to the modelling routine, including slight adjustments to the arrival time of the loading regions, the simulations improved drastically displaying strong correlation with the experimental results. Figure 7 compares the experimental debris field with the simulated debris field from the same viewpoint.

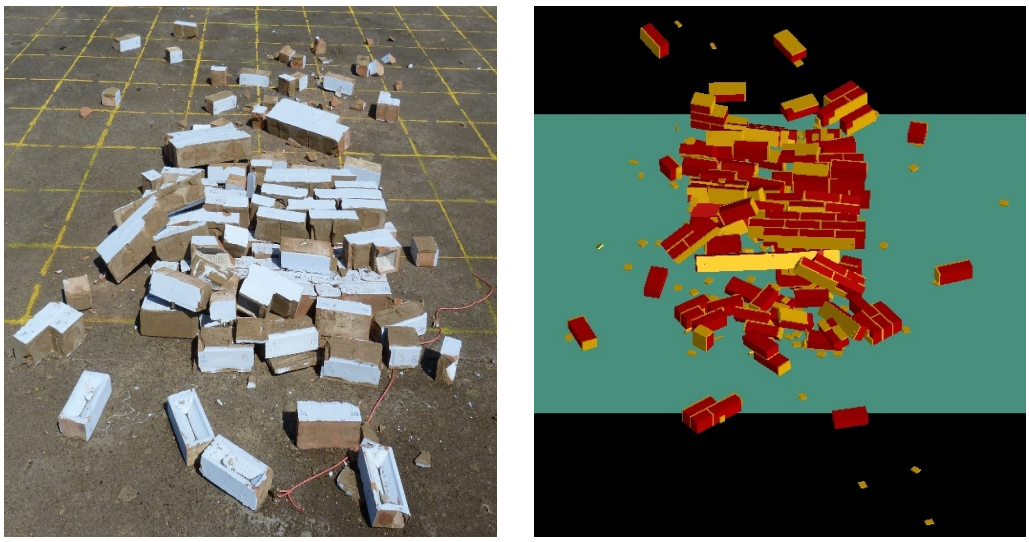

(a) Trial: 41kg at 10.6m **(b)** AEM: 41kg at 10.6m

Figure 7. Comparison of Experimental & Computational Final State Debris Fields

From comparison of Figures 7a and 7b it is clear that the majority of the debris has fallen within the same area. Upon comparison of the mass contained within each individual bin for both the trial and computational model the predictions show varying levels of agreement depending on the position of the bin. The largest discrepancies are seen within close proximity to the original position of the wall, in which there is a 9% difference in mass (as a percentage of the overall mass) as shown in Table 3b. However, upon decreasing proximity to the origin the mass difference per bin becomes small, with the majority of bins showing $\approx 1\%$ discrepancy. Figure 8 displays comparative spatial mass distribution plots of both the trial and AEM model.

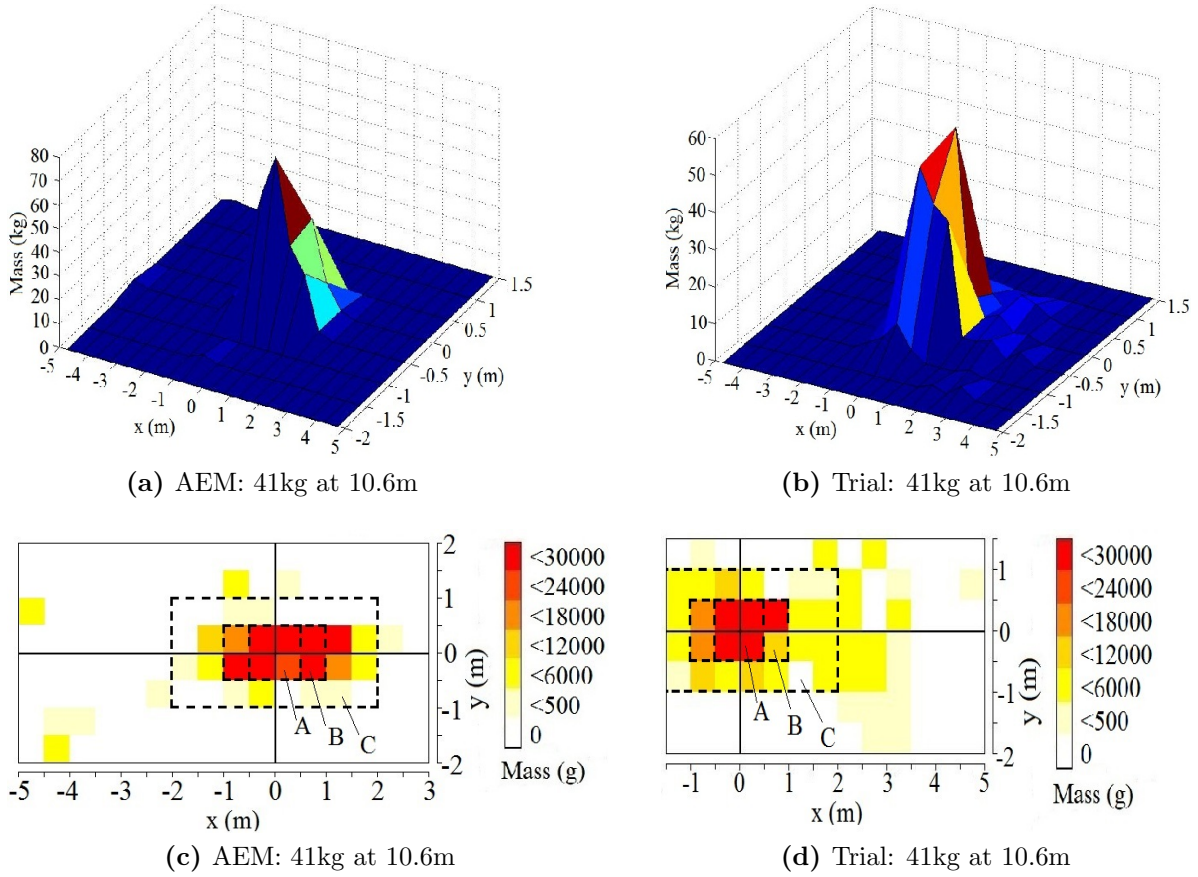

(a) AEM: 41kg at 10.6m

(b) Trial: 41kg at 10.6m

(c) AEM: 41kg at 10.6m

(d) Trial: 41kg at 10.6m

Figure 8. Debris Mass Distribution of 41kg at 10.6m (Normalised to 30kg)

After comparison of the mass contained within each individual bin, the same process can be conducted on a larger scale. Inspection of the mass within localised areas centred around the origin labelled 'A,' 'B' and 'C' as displayed in Figures 8c and 8d gives a clear indication of the difference in debris distribution. Table 3a shows the percentage of the overall mass contained within these areas. The 9% difference in bin mass fell within area A (1m $\times$ 1m); however the overall difference in area A is only 2%. Upon expanding this area to B (2m $\times$ 1m), the difference in the percentage of the overall mass increases to 9%. Finally, increasing the area to C (4m $\times$ 2m) shows a 4% difference in the overall mass.

The model shows varying levels of agreement with the trial data; however when viewed on a larger scale the results are promising. Whilst there is a 9% difference in area B, this is the equivalent to just over 1% per bin. Table 3b shows the average difference per non-zero bin as $\approx 1.4\%$. Figures 7, 8a and 8b display the debris fields of the trial and model in 3D which provides a clear view of the overall debris distribution. When viewed on this scale the potential for AEM to model such events becomes clear.

	Trial	AEM
1m×1m (A)	52%	50%
2m×1m (B)	73%	82%
4m×2m (C)	94%	98%
10m×4m	100%	100%

(a) % of Total Mass within a Localised Area

	All Bins	Bin Mass $\neq 0$
Max	9%	9%
Min	0	$< 0.1\%$
Average	0.5%	1.4%

(b) Variation of Mass per Bin (Trial vs. AEM)

Table 3. Summary Comparison of Experimental and Compuational Mass Distribution

The debris distribution of a structure is greatly dependent on the way in which it fails. Figure 9 shows the breakage patterns displayed by the structure both experimentally and computationally.

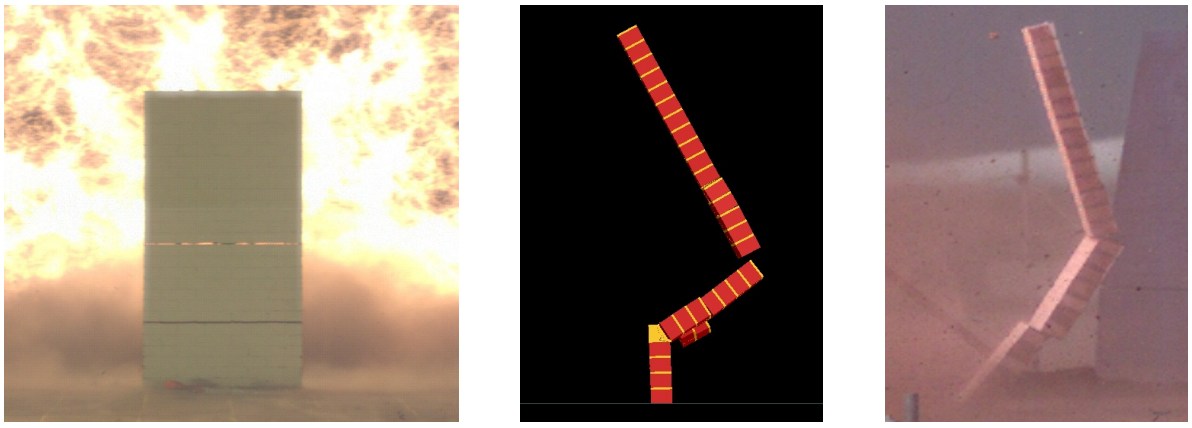

(a) 300ms (rear) **(b)** AEM at 300ms **(c)** 300ms (side)

Figure 9. Comparison of Computational & Experimental Breakage Patterns

Figures 9a, 9b and 9c demonstrate that AEM is capable of matching experimental results to a high degree of accuracy; however, whilst this breakage pattern shows good agreement with that of the experimental breakage pattern, there are small differences which explain the variation in the debris distribution. The bottom quadrant of the wall shows reduced numerical response, whereas the video footage shows the bottom section pivot and fall in the trial; this can cause a longitudinal translation of the debris field. Minor details in the breakage patterns such as this can be reduced further through measured modifications to the modelling routine.

Figure 10 indicates the debris field for the current long duration AEM model which was constructed using only experimental gauge data as represented in Figure 6.

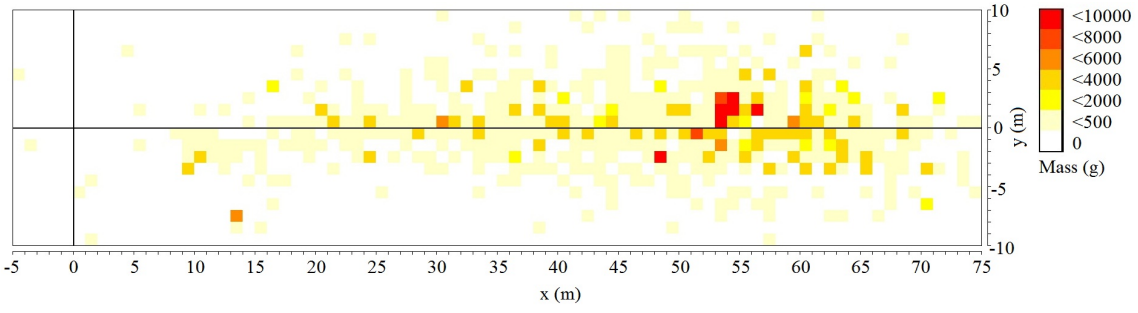

Figure 10. AEM Debris Mass Distribution of 500T at 250m (Normalised to 10kg)

A comparison of Figures 10 and 5a indicates a number of minor challenges pertaining to the absence of a properly resolved flow field. Without being able to resolve the pressure on all sides of the structure or the transferred energy before and after the structure has broken, the simulation models the upper limit of structural failure. The accuracy of the numerical model can be further improved pertaining to additional experimental results and the aid of a CFD simulation. The ability of AEM to accurately model the conventional blast case once a rigid loading routine has been established is further evidence that this is also possible for the long duration case. Adapting the loading regime at the moment of breakage to apply the dynamic pressure and negative phase over the free field pressure will reduce the kinetic energy transferred to the structure.

Summary

AEM has proven to be a powerful tool for modelling the breakage and debris distribution of masonry. The computational models developed for conventional blast, even at this early stage, have thus far shown accurate results. Whilst the model shows varying levels of agreement upon comparison of each bin, comparison of larger areas show more promising results. The debris distribution of the structure is largely determined by its failure mode; thus improvements to the modelling routine will drastically improve the debris distribution. Once a rigid modelling routine has been established for the long duration case, AEM will be used towards a parametric assessment of the breakage and debris distribution of masonry subjected to long duration blast loading.

Nomenclature

Symbols		Subscripts	
I	Impulse	a	Arrival
m	Mass	i	Incident / Free Field
P	Pressure	r	Reflected
Q	Charge Mass (TNT eq.)		
r	Radius Distance	Superscripts	
t	Time	$+$	Positive Phase
μ	Mean		
σ	Standard Deviation		

Acknowledgements

The author would like to express gratitude to the UK Ministry of Defence for providing the use of testing facilities at MoD Shoeburyness. All data hereby obtained through the use of such facilities remains the property of the UK MoD. The assistance of the Spurpark Ltd trials division is gratefully acknowledged with respect to experimental planning, instrumentation and implementation. The author would also like to thank Dr. J. Adams for his oversight and support as well as Dr. T. Rose for his assistance with CFD modelling in Air3D. Finally the author would like to express gratitude to fellow team members Mr. R. Collins and Mr. L. Clough.

References

[1] B. Burgan et al. Buncefield explosion mechanism phase 1. Technical report, Steel Construction Institute, 2009.

[2] G. H. Reid. Misty castle series: Mill race event: Test execution report. Technical report, Defence Nuclear Agency, 1981.

[3] H. Tagel-Din and N. A. Rahman. The applied element method: The ultimate analysis of progressive collapse. April 2006.

[4] Applied Science International LLC, Applied Science International, Durham, North Carolina. *ELS Theoretical Manual*, 2010.

[5] C. N. Kingery and G. Bulmash. Airblast parameters from tnt spherical air burst and hemispherical surface burst. Technical report, 1984.

[6] The British Standards Institution. *BS5628-1:2005 - Code of Practice for the use of Masonry*, 2005. Table 1, page 11.

[7] L. J. Adams et al. Simulating explosive events in the air blast tunnel. 22nd International Symposium on Military Aaspects of Blast and Shock, Bourges, France, November 2012.

[8] T. A. Rose. *An Approach to the Evaluation of Blast Loads on Finite and Infinite Structures*. PhD thesis, Cranfield University, Royal Military College of Science, 2001.